Al-Khwarizmi Engineering Journal, Vol. 4, No. 4, PP 57-70 (2008)

Al-Khwarizmi Engineering Journal

The Effect of Additives on The Performance of Hydrostatic Thrust Bearings

Albert E. Yousif and Muhammed Abdul Sattar

Department of Mechanical Engineering/ College of Engineering/ Nahrain University

(Received 26 September 2007; accepted 13 April 2008)

Abstract

The paper is concerned with, the behavior of the hydrostatic thrust bearings lubricated with liquid-solid lubricants using Einstein viscosity formula, and taking into account the centrifugal force resulting from high speed. Also studied is the effect of the bearing dimensions on the pressure, flow rate, load capacity, shear stress, power consumption and stiffness.

The theoretical results show an increase in load capacity by (8.3%) in the presence of solid graphite particles with concentration of (16%) by weight as compared with pure oil, with increasing shear stress. .

In general the performance of hydrostatic thrust bearings improve for load carrying capacity, volume flow rate, pumping power subjected to centrifugal parameter (S), recess position (r_1), film thickness ratio (β), particle concentration (λ).

Keywords: Thrust Bearings and Liquid - Solid Lubricant.

1. Introduction:

Hydrostatic thrust bearings are finding an increasing use in a wide variety of applications, particularly in machine tools, aerospace industries and large pumps used in pumping storage projects [1].

The fluid or lubricant may be a gas, in the case of pressurized gas bearing but in general high viscosity fluids are used such as oils and water. In recent years many workers studied the effect of contaminants and or polymeric solutions that increase the viscosity index of the lubricant.

In the theory of lubrication, it has been shown that the influence of the inertia terms on the equations of motion is negligible, as compared with effect of the viscous terms, when the Reynolds number Re << 1. Brand [2] carried out an order of magnitude analysis of the equation of motion in thrust bearings. He showed that when Re = 1, the inertia and viscous terms are equally important in predicting the performance characteristics of thrust bearings..

It has been shown by several workers [3-7] that centrifugal forces for bodies of polar symmetry have a significant effect and should be retained in the equations of motions.

The classical theory of hydrostatic lubrication assumes that the lubricant behaves as a newtonian viscous fluid (shear rate varies linearly with the shear stress). However, non-newtonian characteristics have been in variably observed in various processes.

This may be due to the high shear rates and the high pressure gradient, or may be due to additives such as solid lubricants mainly, molybdenum disulfide MoS_2 and graphite. Therefore, the linear relationship between the shear stress and the shear rate is not valid for non-newtonian behavior.

2. Theoretical Analysis:

A circular step thrust bearing is shown in Figure (1) oil from an externally pressurized source is fed to the bearing either through an orifice or a capillary restrictor. The radius of the recess is often appreciable. It enables the static supply pressure to separate the bearing surface.

Dowson [3] assumed that for such bearings the pressure at the lubricant supply hole extends to the step. He also confirmed the validity of the assumption. The theoretical results of Dowson [3] were experimentally corroborated by Coombs and Dowson [8], especially at low speeds.

An approximate expression for the pressure distribution was obtained using the "energy integral method". The validity of applying an energy integral approach was justified by Kapur and Verma [9] who demonstrated the agreement between theoretical and experimental results for magnetohydro-dynamic thrust bearing and squeeze film bearings respectively.

The solid fraction of powder particles contained within base oil is usually taken by weight. This is more acceptable from the physical point of view Einstein equation which takes the following form:

$$\mu^* = \mu_\circ(1+2.5c) \qquad ...(1)$$

where c, represents the volume concentration of the particles, μ^* and $\mu_\circ$ are the viscosity of the suspension and the pure oil, respectively. Furthermore, the constant c, was replaced by a3 in the work of Yousif and Hassan [10], where a3 is postulated by:

$$a^3 = \left(1/(1-1/\lambda)\rho_p/\rho_\circ\right) \qquad ...(2)$$

where, λ is the percentage of the particles by weight. ρ_p and $\rho_\circ$ are the densities of solid particles and oil respectively.

Referring to equ. (2), it can be appreciated that the final form of Einstein formula is a more realistic form than that equation (1) since it deals with the weight rather than volume percentage.

In this paper, the analysis was based on the flow with Einstein's equation as special case in viscosity function:

$$\mu^* = \mu_\circ \Gamma(\lambda) \qquad ...(3)$$

where

$$\Gamma(\lambda) = 1+2.5a^3 \qquad ...(4)$$

3. Governing Equations:

For the externally pressurized circular pad bearing illustrated schematically in Fig.(1) after applying the previous assumptions, the momentum equations can be expressed as follows, taking the centrifugal forces in to account .

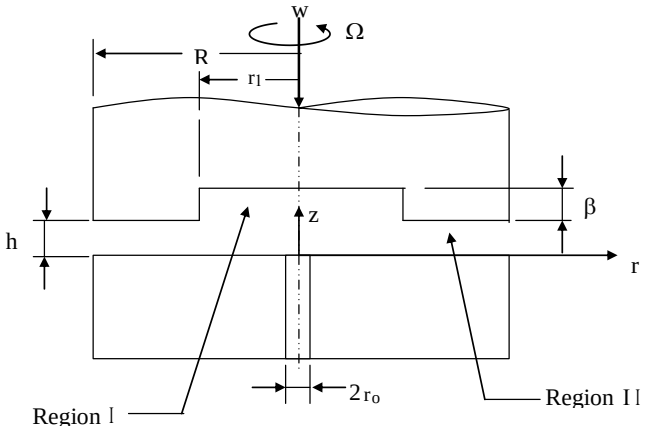

Fig.1. Thrust Hydrostatic Circular Step Bearing.

$$-\frac{\rho v^2}{r} = -\frac{\partial p}{\partial r} + \mu\frac{\partial u^2}{\partial z^2} \qquad ...(5)$$

$$0 = \mu\frac{\partial v^2}{\partial z^2} \qquad ...(6)$$

$$0 = \frac{\partial p}{\partial z} \qquad ...(7)$$

where the variation in pressure in the z-direction is negligible and the equation of continuity is:

$$\frac{1}{r}\frac{\partial(ru)}{\partial r} + \frac{\partial w}{\partial z} = 0 \qquad ...(8)$$

The simplified momentum equations, in dimensionless form, reduce to:

$$-\frac{S\bar{v}^2}{\bar{r}} = -\frac{\partial \bar{p}}{\partial \bar{r}} + \frac{1}{\delta}\frac{\partial^2 \bar{u}}{\partial \bar{z}^2} - \frac{k}{\delta}\frac{\partial^4 \bar{u}}{\partial \bar{z}^4} \qquad ...(9)$$

$$0 = \frac{\partial^2 \bar{v}}{\partial \bar{z}^2} - k\frac{\partial^4 \bar{v}}{\partial \bar{z}^4} \qquad ...(10)$$

$$0 = \frac{\partial \bar{p}}{\partial \bar{z}} \qquad ...(11)$$

and the equation of continuity is:

$$\frac{\partial \bar{u}}{\partial \bar{r}} + \frac{\bar{u}}{\bar{r}} + \frac{\partial \bar{w}}{\partial \bar{z}} = 0 \qquad ...(12)$$

where $k = \eta/\mu * R2$,
$\delta = Pr/\mu * \Omega$,
$S = \rho\Omega^2 R^2 / P_r$

The volume flow rate $\overline{Q}$ can be evaluated from the integral

$$\overline{Q} = \int_0^{\beta\overline{h}} 2\pi r \overline{u} d\overline{z} \qquad ...(13)$$

The velocity distribution without centrifugal effects, by integrating equ.(9) and applying boundary conditions that the radial velocity on the upper and lower surfaces of the bearing, satisfy equ. (12) is obtained as:
The boundary conditions are:

$$\begin{aligned} &\overline{u} = 0 \quad \text{at} \quad \overline{z} = 0 \\ &\overline{u} = 0 \quad \text{at} \quad \overline{z} = \beta\overline{h} \qquad ...(14) \\ &\frac{\partial^2 \overline{u}}{\partial \overline{z}^2} = 0 \quad \text{at} \quad \overline{z} = 0 \\ &\frac{\partial^2 \overline{u}}{\partial \overline{z}} = 0 \quad \text{at} \quad \overline{z} = \beta\overline{h} \end{aligned}$$

The velocity v can be found by integrating equ. (10) twice, subject to the boundary conditions that,

$$\begin{aligned} &\overline{v} = 0 \quad \text{at} \quad \overline{z} = 0 \\ &\overline{v} = \overline{r} \quad \text{at} \quad \overline{z} = \beta\overline{h} \qquad ...(15) \\ &\frac{\partial^2 \overline{v}}{\partial \overline{z}^2} = 0 \quad \text{at} \quad \overline{z} = 0, \beta\overline{h} \end{aligned}$$

Thus, it can be shown that:

$$\overline{v} = \frac{\overline{r}\,\overline{z}}{\beta\overline{h}} \qquad ...(16)$$

4. Pressure Distribution:

The radial pressure gradient is obtained from equation (9) by applying an energy integral approach [9]. Multiplying equation (9) by u and integrating the resulting expression can be obtain as follows:

$$\frac{\partial \overline{p}}{\partial \overline{r}} \int_0^{\beta\overline{h}} \overline{u} d\overline{z} = \frac{S}{\overline{r}} \int_0^{\beta\overline{h}} \overline{u}\,\overline{v}^2 d\overline{z} + \frac{1}{\delta} \int_0^{\beta\overline{h}} \overline{u} \frac{\partial^2 \overline{u}}{\partial \overline{z}^2} dz \quad ...(17)$$

$$\frac{\partial \overline{p}}{\partial \overline{r}} = \frac{S f_2(\beta\overline{h})}{(\beta\overline{h})^2 f_1(\beta\overline{h})} \overline{r} + \frac{\overline{Q}\Gamma(\lambda)}{f_1(\beta\overline{h})} \frac{1}{\overline{r}} \qquad ...(18)$$

where

$$f_2(\beta\overline{h}) = -\frac{(\beta\overline{h})^3}{6}$$

$$f_2(\beta\overline{h}) = -\frac{(\beta\overline{h})^5}{20}$$

For a bearing of the form shown in fig.1 expressions for the pressure distribution on the either side of the step are required. The pressure distribution takes the forms:
For region I (recess) Fig.1 : $\overline{r}_\circ \le \overline{r} \le \overline{r}_1$

$$\overline{P} = \frac{S f_2(\beta\overline{h})}{2(\beta h)^2 f_1(\beta\overline{h})} \overline{r}^2 + \frac{\overline{Q}\Gamma(\lambda)}{f_1(\beta\overline{h})} \ln \overline{r} + c_1$$

where c_1 is constants of integration.
The boundary conditions are:

$$\overline{P} = 1 \quad \text{at} \quad \overline{r} = \overline{r}_\circ \quad \text{and} \quad h = \beta\overline{h}$$

Hence,

$$\overline{P} = 1 + \frac{S f_2(\beta\overline{h})}{2(\beta h)^2 f_1(\beta\overline{h})} \left(\overline{r}^2 - \overline{r}_\circ^2\right) + \frac{\overline{Q}\Gamma(\lambda)}{f_1(\beta\overline{h})} \ln\left(\frac{\overline{r}}{r_\circ}\right)$$

...(19)
For region II (land) Fig.1: $\overline{r}_1 \le \overline{r} \le 1$

$$\overline{P} = \frac{S f_2(\overline{h})}{2(\overline{h})^2 f_1(\overline{h})} \overline{r}^2 + \frac{\overline{Q}\Gamma(\lambda)}{f_1(\overline{h})} \ln \overline{r} + c_2$$

where c_2 is constant of integration.
The boundary conditions are:

$$\overline{P} = 0 \quad \text{at} \quad \overline{r} = 1 \quad \text{and} \quad h = \overline{h}$$

Hence,

$$\overline{P} = \frac{S f_2(\overline{h})}{2\overline{h}^2 f_1(\overline{h})} \left(\overline{r}^2 - 1\right) + \frac{\overline{Q}\Gamma(\lambda)}{f_1(\overline{h})} \ln \overline{r} \qquad ...(20)$$

5. Lubricant Flow Rate:

Assuming pressure continuity at the step, then from equations(18) and (20)the dimensionless flow rate is obtained as:

$$\overline{Q}=\frac{\left(1+S\left(\frac{f_2(\beta\bar{h})(\bar{r}_1^2-\bar{r}_\circ^2)}{2(\beta\bar{h})^2 f_1(\beta\bar{h})}-\frac{f_2(\bar{h})}{2(\bar{h}^2)f_1(h)}(\bar{r}_1^2-1)\right)\right)}{\left(\frac{\ln r_1}{f_1(\bar{h})}-\frac{\ln\frac{\bar{r}_1}{r_\circ}}{f_1(\beta\bar{h})}\right)\Gamma(\lambda)} \quad ...(21)$$

6. Load-Carrying Capacity:

The dimensionless load-carrying capacity $\overline{w}$, of the bearing considered above, can be calculated as:

$$\overline{W}=\bar{r}_\circ^2+2\int_{\bar{r}_\circ}^{\bar{r}_1}\bar{r}\,\bar{p}\,d\bar{r}+2\int_{\bar{r}_1}^{1}\bar{r}\,\bar{p}\,d\bar{r} \quad ...(22)$$

Hence, the result is expressed as:

$$\overline{W}=\bar{r}_\circ^2+\overline{W}_1+\overline{W}_2 \quad ...(23)$$

where $\overline{W}_1$ and $\overline{W}_2$ are the load capacities in the regions of recess ($\bar{r}_\circ\le\bar{r}\le\bar{r}_1$) and (land) ($\bar{r}_1\le\bar{r}\le 1$) respectively, such that:

$$\overline{W}_1=\frac{1}{4}\bar{r}_1^2\left(\frac{4(\beta\bar{h})^2 f_1(\beta\bar{h})+4\overline{Q}\ln\left(\frac{\bar{r}_1}{\bar{r}_\circ}\right)(\beta h)^2-2\overline{Q}(\beta\bar{h})^2+Sf_2(\beta\bar{h})\bar{r}_1^2-2Sf_2(\beta h)\bar{r}_\circ^2}{(\beta^2 h^2 f_1(\beta\bar{h}))}\right)$$

$$-\bar{r}_\circ^2-\frac{1}{4}\bar{r}_\circ^2\left(\frac{-2\overline{Q}(\beta\bar{h})^2-Sf_2(\beta\bar{h})\bar{r}_\circ^2}{(\beta\bar{h})^2 f_1(\beta\bar{h})}\right) \quad ...(24)$$

$$\overline{W}_2=-\frac{1}{4}\left(\frac{Sf_2(h)+2\overline{Q}\bar{h}^2+\bar{r}_1^4-Sf_2(\bar{h})-2\bar{r}_1^2\overline{Q}\bar{h}^2-}{\bar{h}^2.f_1(h)}+\frac{2Sf_2(h)\bar{r}_1^2+4\bar{r}_1^2\overline{Q}\ln(\bar{r}_1)\bar{h}^2}{\bar{h}^2.f_1(h)}\right) \quad ...(25)$$

7. Bearing Power Consumption:

There are two contributions to bearing power losses:

1. The power lost due to pad rotation.
2. Losses due to pumping the lubricant through the bearing clearance.

The power loss due to pad rotation is obtained as follows. If the bearing components move relative to each other the frictional resistance to such motion is due to the force required to shear the lubricant. The shear stress for this case is:

$$\tau_\theta=\mu^*\left(\frac{\partial v}{\partial z}\right)_{z=h}$$

When the expression for the tangential velocity (v) given in equ. (14) is used, the frictional drag on an element of area (2πrdr) is given by:

$$dF=2\pi\cdot r\cdot\tau\cdot dr \quad ...(26)$$

or

$$dF=2\pi\mu^*\frac{\pi r^2}{\beta h}dr \quad ...(27)$$

and the frictional torque on the element is:

$d\Im$= r.dF

or

$$d\Im=2\pi\mu^*\frac{\pi r^3}{\beta h}dr$$

The frictional torque $\Im$ is obtained by integrating the elemental torque over the bearing area:

$$\Im=2\pi\mu^*\Omega\left\{\int_{r_\circ}^{r_1}\frac{r^3}{\beta h}dr+\int_{r_1}^{R}\frac{r^3}{h}dr\right\} \quad ...(28)$$

The frictional power Pf is defined as:

$$\text{Pf}=\Im\Omega=\frac{\pi\mu^*\Omega^2}{2}\left\{\left(\frac{r_1^4-r_\circ^4}{\beta h}\right)+\left(\frac{R^4-r_1^4}{h}\right)\right\} \quad ...(29)$$

The pumping power required to operate the bearing can be expressed as:

Pp=Q.Ps …(30)

The power factor is:

$$H_f=\frac{\overline{Q}}{\overline{W}^2} \quad ...(31)$$

8. Stiffness:

The bearing stiffness can be expressed

$$\alpha = -\pi R^2 P_s \overline{w} \frac{dkp}{dh} \qquad ...(32)$$

The flow through the restrictor can be written in a general form as:

$$Q_i = k_Q h^q P_s^n \left(1-k_p\right)^n \qquad ...(33)$$

where kQ, q and n are the compensator flow constants.

Using equs. (21) and (33) and differentiation of the resulting equation with respect to h one gets:

$$\frac{dk_p}{dh} = \left\{ \frac{-\left(\frac{k_p^2}{k_Q}\frac{dk_s}{dh}\right)}{\left(1-k_p\right)^n\left[\frac{nk_p}{\left(1-k_p\right)}+1\right]} \right\} \qquad ...(34)$$

Where

$$\overline{Q_\circ} = k_s k_p$$

$$k_s = -\frac{\pi P_s R^3}{6\mu}\left[\frac{1+\frac{3}{20}S\left(1-r_\circ^2\right)}{\ln r_1 - \left(\ln\frac{r_1}{r_\circ}/\beta^3\right)}\right]h^3 \qquad ...(35)$$

The stiffness per unit supply pressure (Ss) is defined in dimensionless form as:

$$S_s = \frac{\alpha h}{P_s A} \qquad ...(36)$$

9. Results and Discussion:

Results are presented in terms of dimensionless pressure distribution $\overline{P}$, load carrying capacity $\overline{W}$, flow rate $\overline{Q}$, stiffness per unit supply pressure S_S, shear stress τ_w, centrifugal parameter S, solid particle concentration λ. The viscosity for pure oil at atmospheric pressure $\left(\mu_o = 0.04\ Pa.s\right)$ SAE 30 at 50 Co, density of the oil (ρ = 850 Kg/m^3), Table (1) shows type of solid particle since the Non-Newtonian behavior of the liquid solid lubricant is attributed to the existence of these solid particles where (CO) uniaxial compressive strength (N/m^2).

Table 1
Properties of The Most common Solid Lubricants

Solid lubricant	Co (N/m^2)	EP (N/m^2)	ρp (kg/m^3)	νp
MoS_2	3.2E10	2.8E9	4800	0.31
Carbon graphite	2.7E10	2.8E8	1730	0.3
Teflon	7E8	2.8E8	2160	0.3

The bearing radial direction is divided into two main parts, the first region is in the recess $\left(\bar{r}_o \le \bar{r} \le \bar{r}_1\right)$ and second region is in the land $\left(\bar{r}_1 \le \bar{r} \le 1\right)$ to study the simultaneous influence of solid particle concentration λ and centrifugal parameter S on the performance of hydrostatic thrust bearing.

Fig. (2)-(5) show the variation at different positions for various values of the parameters such as solid particle concentration λ, centrifugal parameter S, film thickness ratio β, couple stress parameter τ, and recess radius $\bar{r}_1$.

Fig. (2) and Fig. (3) represent the theoretical pressure distribution increasing with increase the centrifugal parameter S when increase rotating speed (Ω) and film thickness ratio (β) because of increase in pocket pressure for pure oil. These results is in agreement with Dowson's[3].

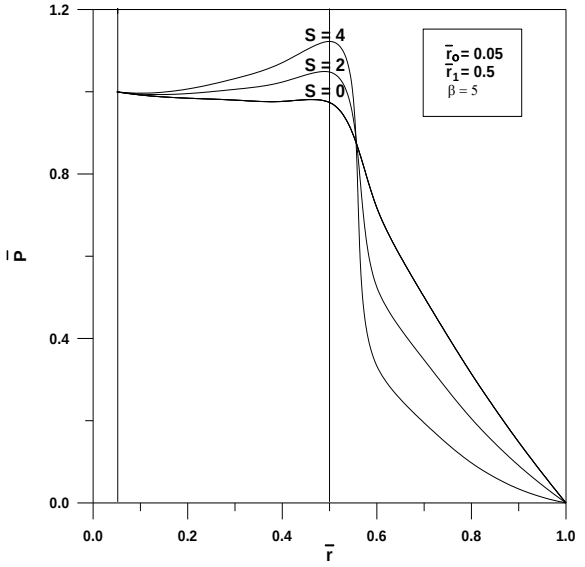

Fig. 2. Effect of Centrifugal Parameter (S) on the Pressure Distribution for Pure Oil.

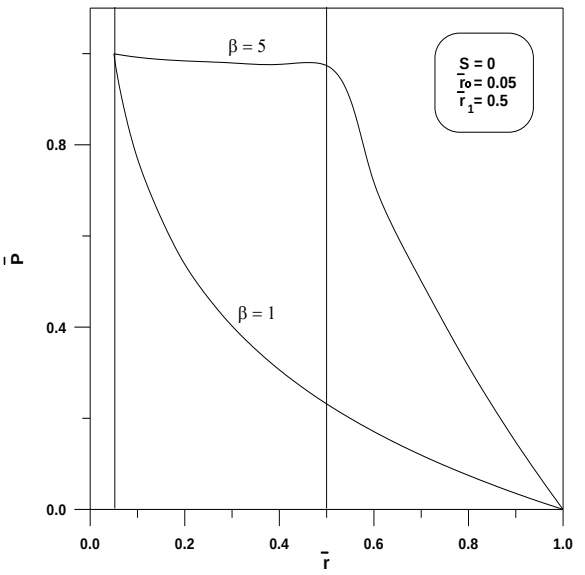

Fig.3. Effect of the Film Thickness Ratio (β) on the Pressure Distribution for Pure Oil.

Fig. (4) represent effect of increasing the recess radius $\bar{r}_1$ over the pressure distribution for pure oil because of increase in pocket area.

Fig. (5) shows the pressure minus, if recess is less than 0.3, a negative pressure region will appear on the bearing land and cavitation may occur, for increasing rotating speed Ω has a beneficial effect on the pressure distribution if $(\bar{r}_1 \geq 0.3)$, but it is deleterious if $(\bar{r}_1 \leq 0.3)$ because the negative pressure region in the bearing land increases with increasing rotating speed Ω which may lead to cavitation.

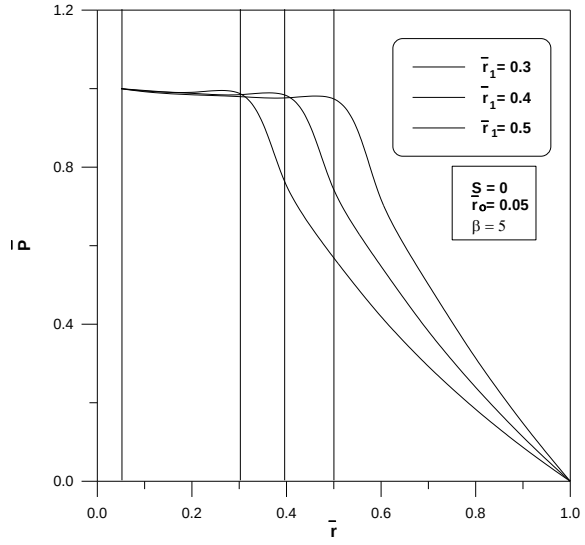

Fig. 4. Effect of the Recess Radius (r_1) on the Pressure Distribution for Pure Oil.

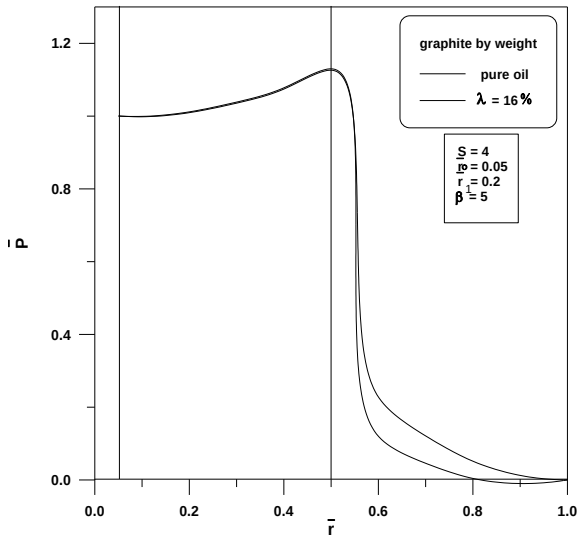

Fig. 5. Effect of the Solid Concentration (λ) on the Pressure Distribution to Avoid Minus Pressure.

In this work the results of additives of solid particle (lubricant with contaminant) we can avoid cavitation this case is shown in figure (5) when increasing concentration of solid particle λ the pressure negative reduced.

The pressure gradient changes sign at a point along the flow where the viscous and inertia forces are equal. The position of this point depends on Ω, β, λ and $\bar{r}_1$.

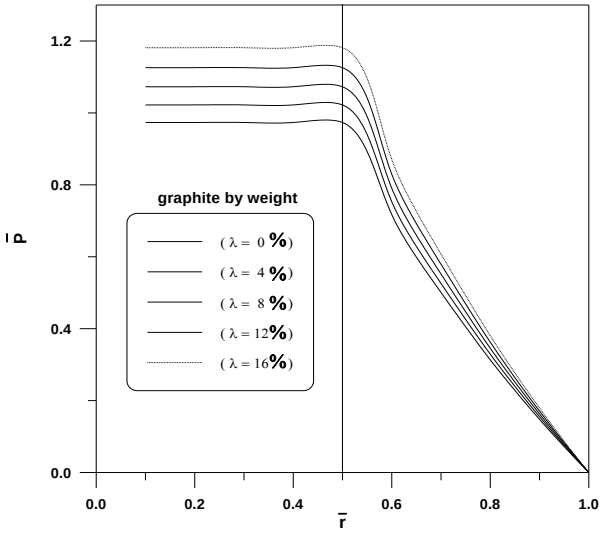

Fig. 6. Effect of the Concentration of Solid Particles (λ) on the Pressure Distribution in the Absence of the Hole of Radius r_o.

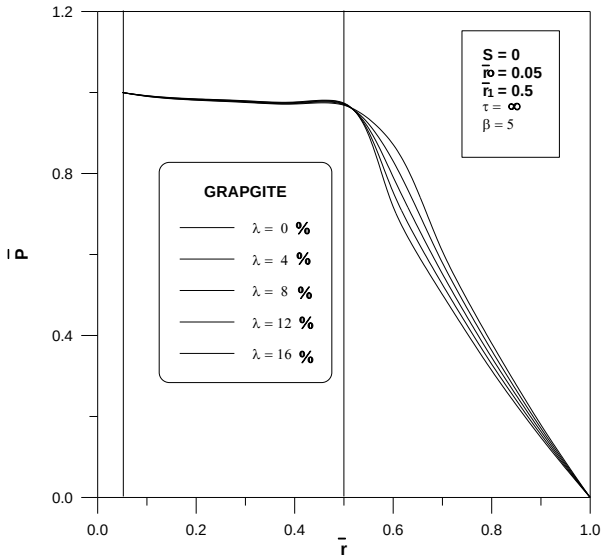

Fig.7. Effect the Concentration of Solid Particles (λ) on the Pressure Distribution.

Fig.(6) and Fig. (7) represent the concentration of solid particle λ effect on the pressure distribution without effect of the hole radius $\bar{r}_o$. This result shows increase in the recess region and land region by using boundary condition in recess, when the pressure is constant see [15], but in this research boundary condition involves the hole radius $\bar{r}_o$. Hence, the pressure at this case can be represented in Fig. (7).

Fig. (8) represents the effect of solid particle concentration λ on the pressure distribution of the three types of solid particle used, graphite has higher effect than MoS2 and Teflon. The increase in density of the addition the viscosity for mixture increases by effect on the formula $\Gamma(\lambda)$.

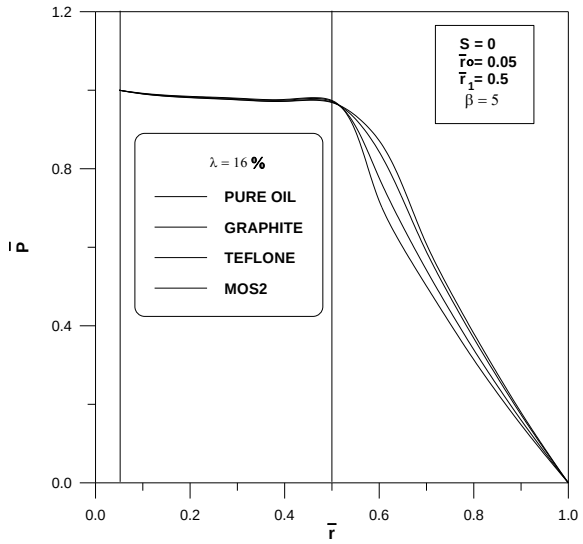

Fig. 8. Effect of the Type of Solid Concentration Particle (λ) on the Pressure Distribution.

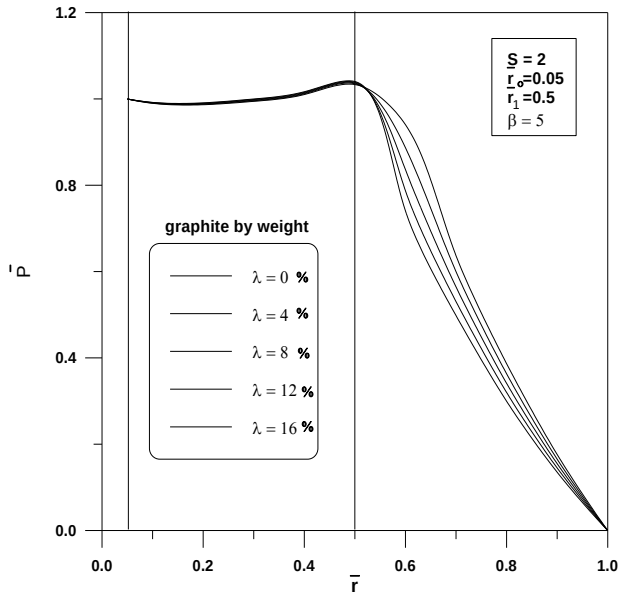

Fig. 9. Effect the Concentration of Solid Particles (λ) on the Pressure Distribution.

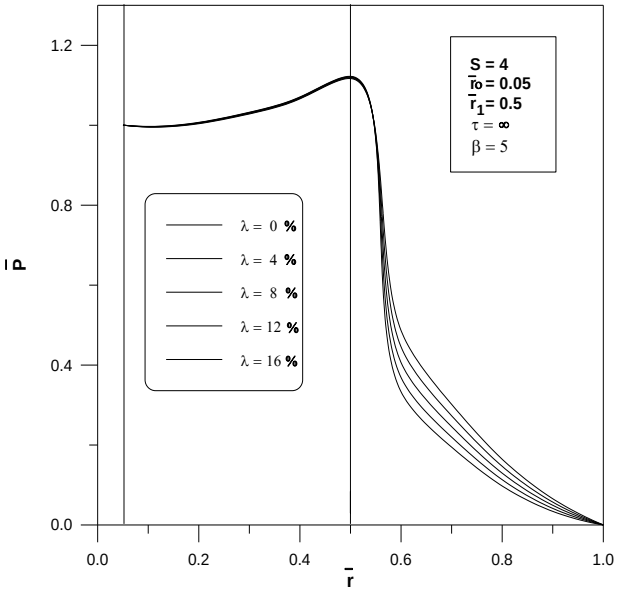

Fig. 10. Effect the Concentration of Solid Particles (λ) on the Pressure Distribution.

Fig. (9) and Fig. (10) show the pressure distribution increasing with increase solid particle concentration λ with (S=0, S=2, S=4) and $\bar{r}_1 = 0.5$.

9.1. Volume Flow Rates ($\overline{Q}$):

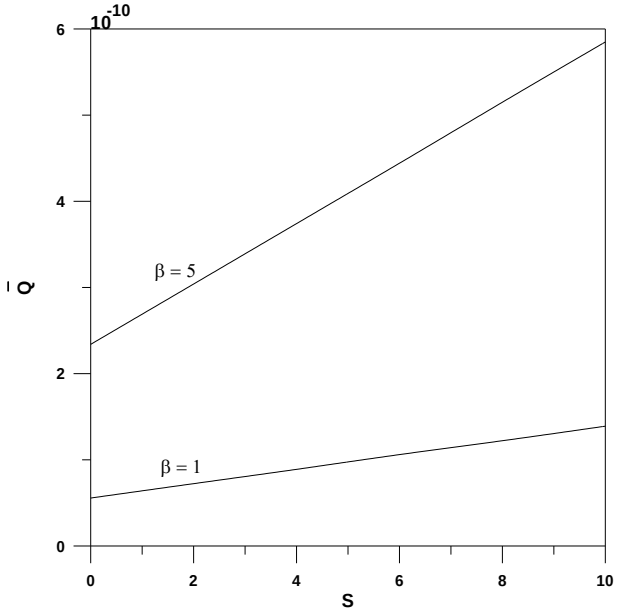

Fig. 11. Variation of the Flow Rate (Q) With Centrifugal Parameter (S) and Film Thickness Ratio (β).

Fig. (11) shows that the flow rates $\overline{Q}$ increases with increasing centrifugal parameter S and film thickness ratio β.

Fig. (12) shows the effect of solid particle concentration λ for graphite and MoS2 and recess radius $\bar{r}_1$. The flow increases with increase of recess radius $\bar{r}_1$ because of increase in pocket area and decreases with increasing solid particle concentration λ because of increase in viscosity.

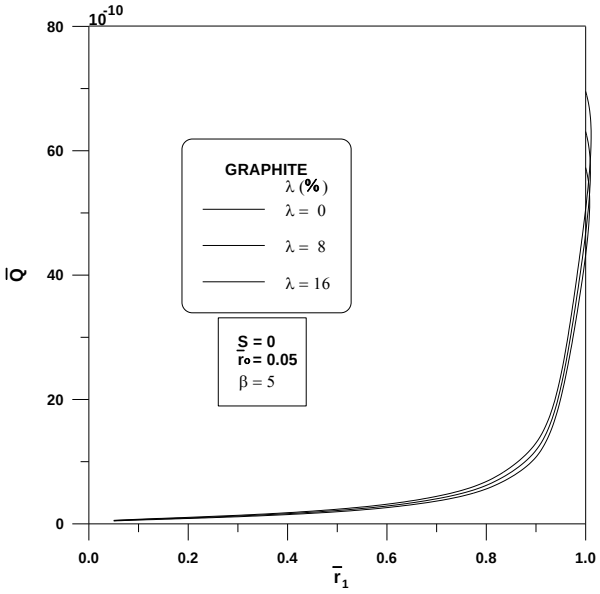

Fig. 12. Variation in Flow Rate (Q) With Recess Position (r_1).

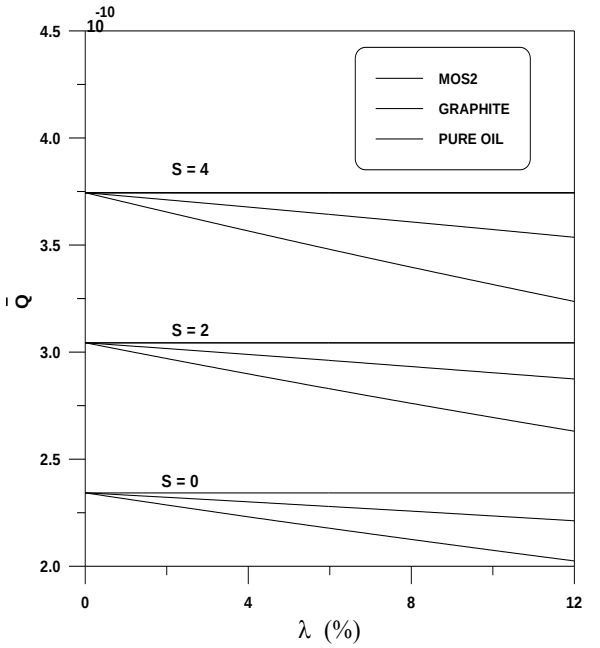

Fig. 13. Variation in Flow Rate (Q) Withthe of Solid Particle Concentration (λ).

Fig. (13) shows variation of flow rate $\overline{Q}$ with solid particle concentration λ for graphite and MoS2, flow rate $\overline{Q}$ decreases with increasing solid particle concentration λ.

9.2. Load Carrying Capacity ($\overline{W}$):

Fig. (14) shows the variation of load carrying $\overline{W}$ with recess radius $\bar{r}_1$ and centrifugal parameter S. Load carrying $\overline{W}$ increases with increase recess radius $\bar{r}_1$ and centrifugal parameter S. These results are similar to those reported by Dowson [3] where the classical viscous fluid theory (pure oil) was used.

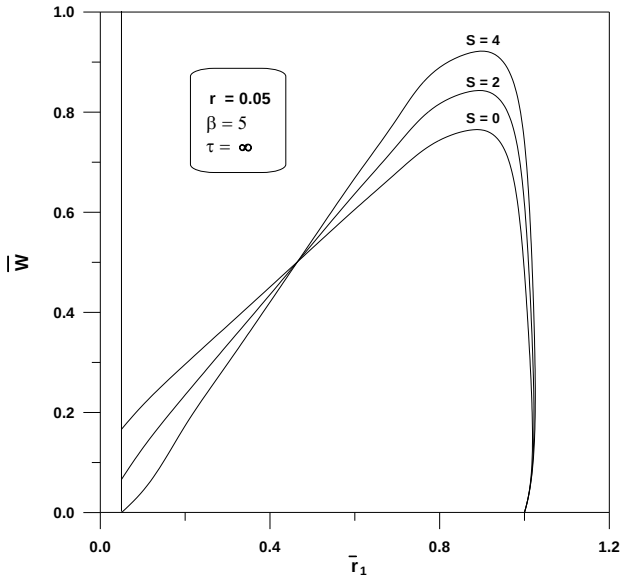

Fig.14. Effect of Recess Radius Ratio ($\bar{r}_1$) Andcentrifugal Parameter (S) on the Load Factor($\overline{W}$).

Fig.(15) shows that increasing load capacity increases with increasing solid particle concentration λ, load carrying capacity is higher for graphite than for Teflon and MoS_2 because of increasing in viscosity.

Fig. (16) shows increase in load capacity with increase in solid particle concentration and recess radius because of increase in pocket area by increase recess radius.

Load carrying capacity increase by 8.3% for solid particle concentration of 16% graphite by weight as compared with pure oil. When using couple stresses fluid load carrying capacity increased by 9.7% for solid particle concentration of 16% graphite by weight as compared with pure oil.

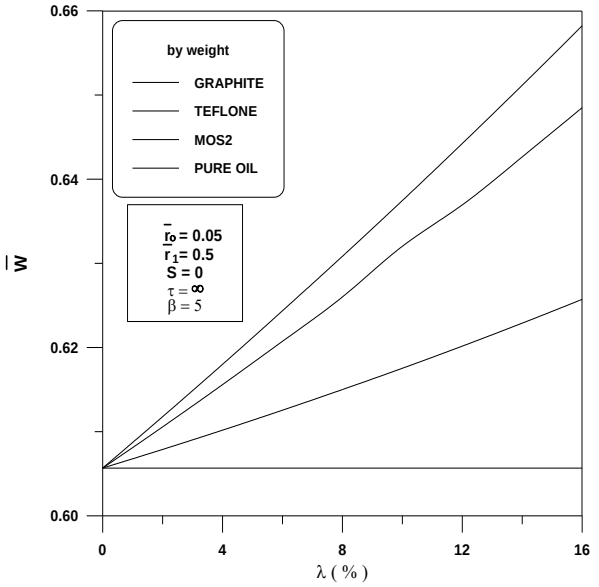

Fig.15. Variation of the Load Factor ($\overline{W}$) With Three Type of Solid Particle Concentration (λ).

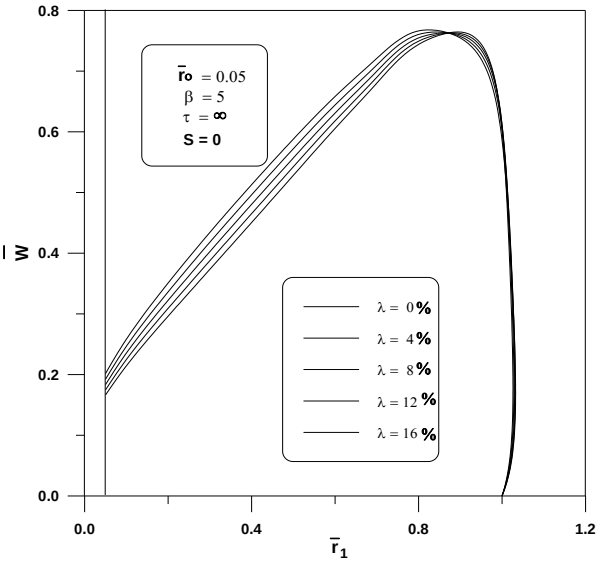

Fig.16. Effect of Recess Radius Ratio ($\bar{r}_1$) and Concentration of Solid Particle (λ) on the Load Factor (w).

9.3. Power Factor (H_P):

Fig. (17) shows the effect of recess radius $\bar{r}_1$ and centrifugal parameter S on the power factor H_P for pure oil. It can be stated that as $\bar{r}_1$ increases from 0.05 to 0.9, power factor H_P

decreases until it reaches a minimum value at certain $\bar{r}_1$ and then H_P increases as $\bar{r}_1$ increases. The value of $\bar{r}_1$ at which H_P is a minimum depends on S, i.e. as S increases from 2 to 4. The value of $\bar{r}_1$ at minimum H_P increases. It is also clear that as S increases from 0 to 2, H_P decreases and as S increases from 2 to 4, H_P may increase or decrease depending on the value of $\bar{r}_1$. The results are in agreement with those Khalil and Ismail [15].

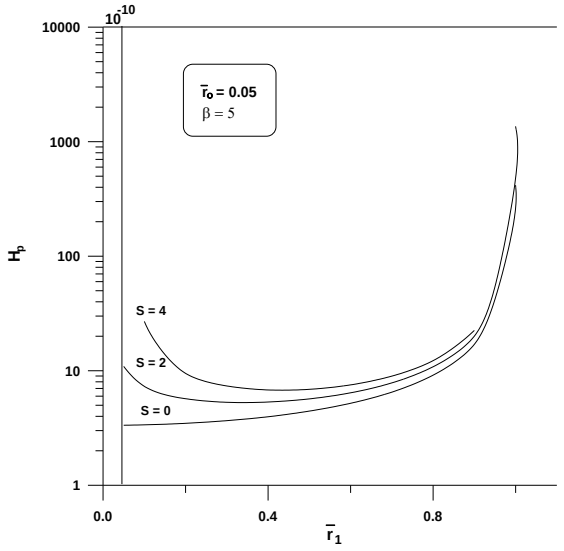

Fig.17. Effect of Recess Radius Ratio ($\bar{r}_1$) and Centrifugal Parameter (S) on the Power Factor(H_p).

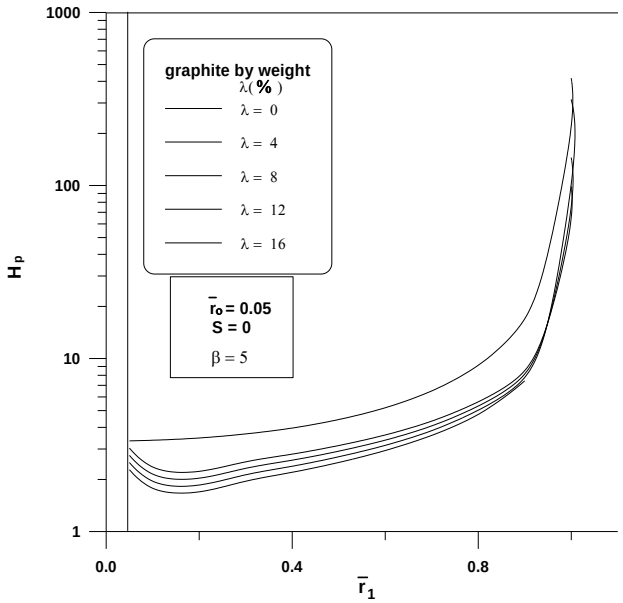

Fig. 18. Effect of Recess Radius Ratio ($\bar{r}_1$) and Solid Particle Concentration (λ) on the Power Factor (H_p).

Fig. (18) shows the effect of concentration of the solid particle λ (graphite by weight) on the power factor H_P. It is clear that the power factor H_P decreases when solid particle concentration λ increases with recess radius $\bar{r}_1$ (0.05 to 1).

9.4. Stiffness Per Unit Supply Pressure (S_S):

Fig. (19) shows the effect of compensation (orifice and capillary) and recess radius $\bar{r}_1$ on the stiffness per unit supply pressure S_S. The ratios K_P and β are taken as 0.5 and 5 respectively. It is clear that as recess radius $\bar{r}_1$ increases from 0.05 to 0.9 stiffness factor S_S increases. However, the orifice compensation is stiffer than the capillary compensation.

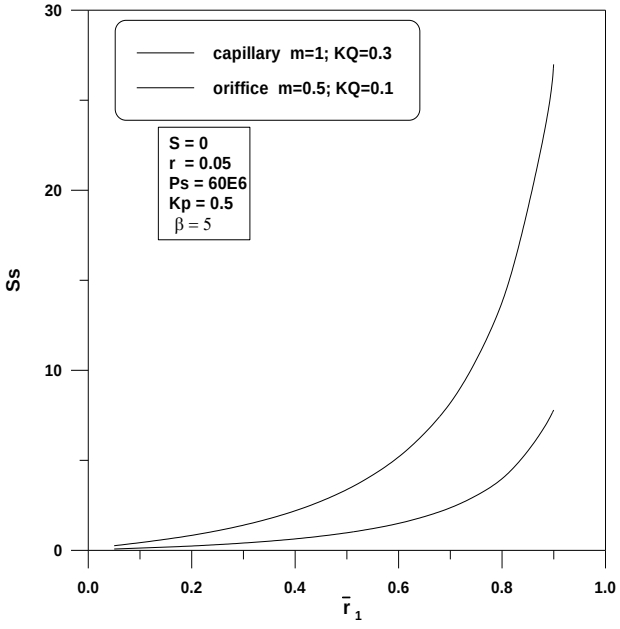

Fig. 19. Effect of Recess Radius Ratio ($\bar{r}_1$) on the Stiffness Factor (S_S) for (Capillary and Orifice) Compensation.

Fig. (20) shows the effect of the solid particle concentration λ, the ratio K_P varying from 0.1 to 0.9 and with values of β take 5, the recess radius $\bar{r}_1$ is taken as 0.6. It clear that S_S increases with increasing solid particle concentration λ .Graphite increases the stiffness per unit supply pressure S_S more than MoS2 because of its higher density,

hence causing an increase in the viscosity of the mixture.

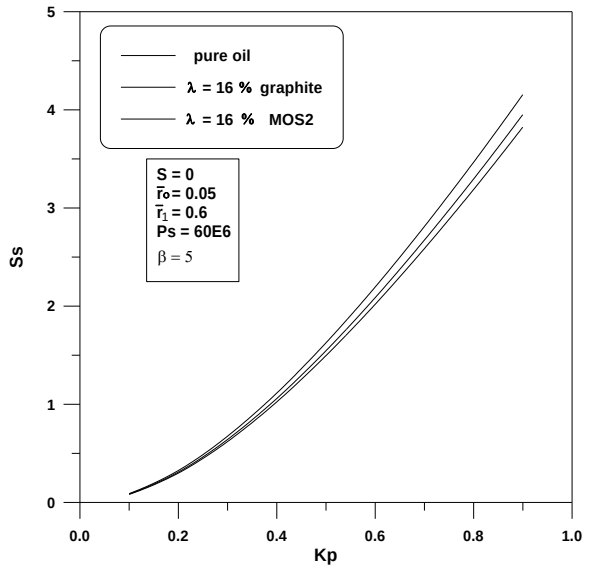

Fig.20. Effect of the Solid Particle Concentration (λ) and Pressure Ratio (K_P) on the Stiffness Factor (S_S).

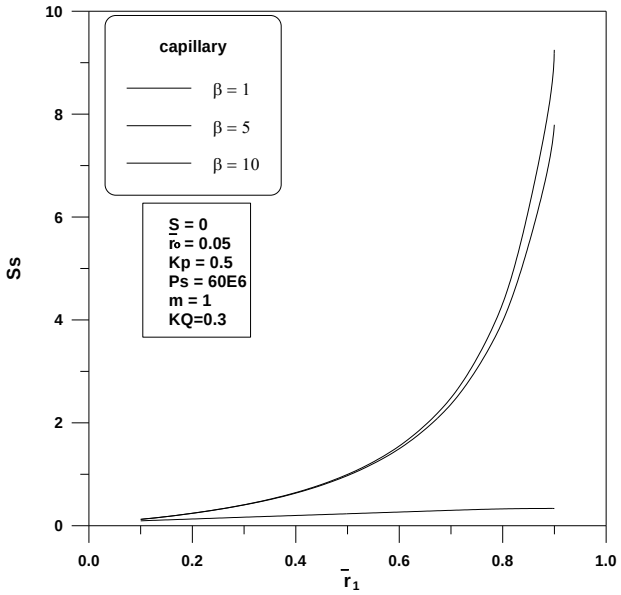

Fig.21. Effect of Film Thickness Ratio (β) on the Stiffness Factor (S_S).

Fig. (21) shows the effect of film thickness ratio β on the stiffness factor S_S, recess radius $\bar{r}_1$ has range from 0.1 to 0.9, the ratio KP takes 0.5. It is clear that S_S increases when β increases for capillary compensation.

Fig. (22) shows the effect of the centrifugal parameter S on the stiffness factor S_S. It is clear that when centrifugal parameters S increases stiffness factor S_S increases because of increasing rotating speed Ω, hence increase load carrying capacity.

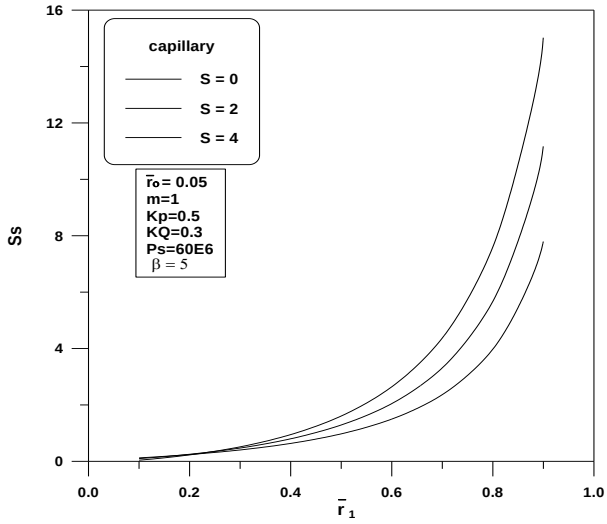

Fig. 22. Effect of Centrifugal Parameter (S) on the Stiffness Factor (S_S).

9.5. Frictional Power Fp:

Fig. (23) show the frictional power Fp variation with different values of film h and Fig. (24) show solid particle concentration λ effect on the frictional power Fp. The frictional power decreases with film thickness h and increases with increase in solid particle concentration λ because of increase in viscosity.

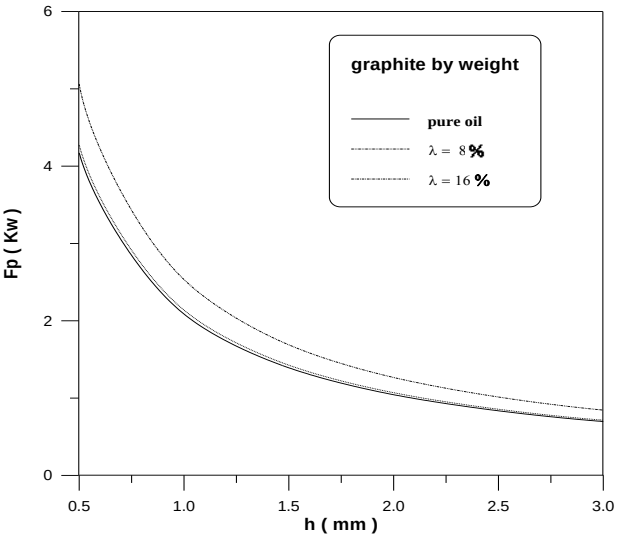

Fig. 23. Effect of Solid Particle Concentration (λ) on the Frictional Power (F_P) (μ=0.04Pa.s, β=5, r_1=0.5m, Ω=100rpm, R=1m).

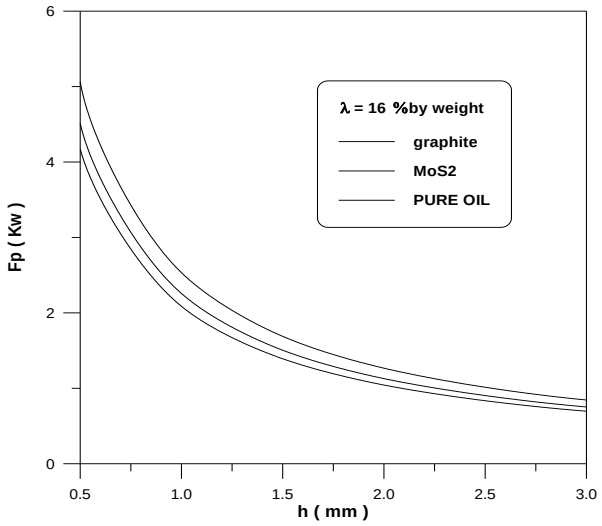

Fig.24. Effect of Solid Particle Concentration (λ) on the Frictional Power (μ=0.04Pa.s, β=5, r_1=0.5m, Ω=100rpm, R=1m).

Fig.(25) shows the frictional power Fp increases with increase in recess radius $\bar{r}_1$.

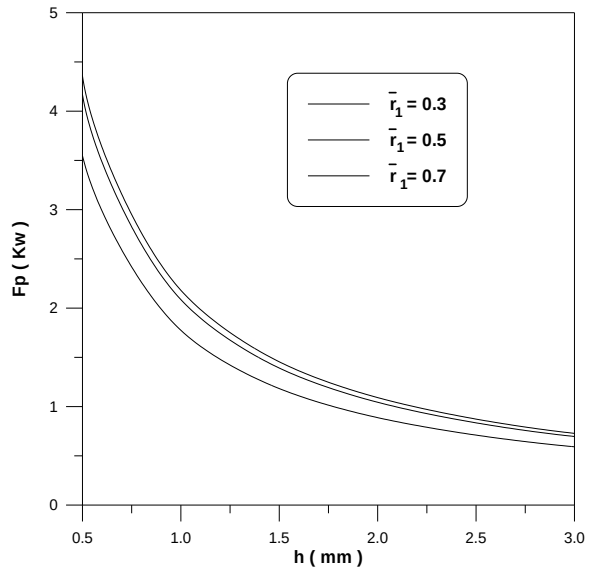

Fig. 25. Effect of Recess Radius ($\bar{r}_1$) on the Frictional Power (F_P) (μ=0.04Pa.s, β=5, Ω=100rpm, r_o=0.05m, R=1m).

Fig. (26) shows the effect of rotating speed Ω on the frictional power factor Fp, it increases with increase in rotating speed Ω.

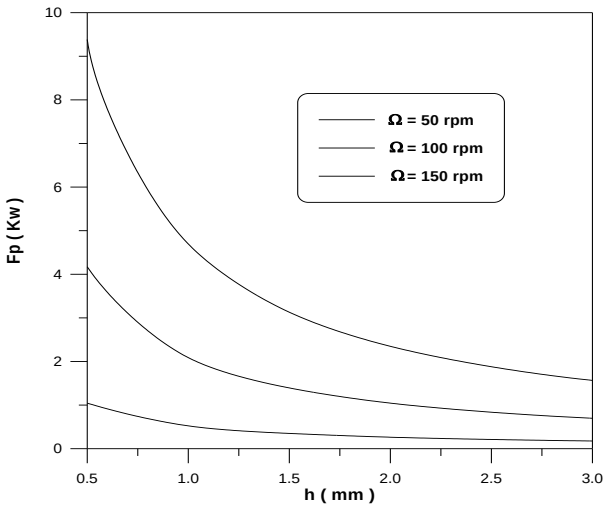

Fig.26. Effect of Rotating Speed (Ω) on the Frictional Power (F_P) (μ=0.04Pa.s, β=5, r_1=0.5m, r_o=0.05m, R=1m).

9.6. Shear Stress (τ_w):

Fig.(27) shows the effect of solid particle concentration λ on shear stress τ_w, it is clear that shear stress τ_w increases with increase in solid particle concentration.

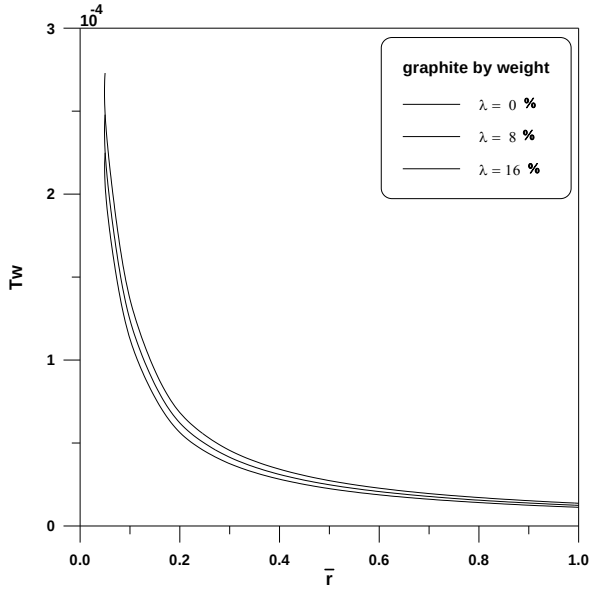

Fig.27. Effect of Solid Particle Concentration (λ) on the Shear Stress (τ_w).

10. Nomenclatures:

R	Outside radius of bearing
r / R	dimensionless radial radius
$\bar{r}_1$ r_1 / R	dimensionless radius of step
$\bar{r}_o$ r_o / R	dimensionless hole radius
$\bar{Z}$ z / R	dimensionless axial coordinate
$\bar{h}$ h / R	dimensionless film thickness
β	Film thickness ratio
Ω	Angular speed rev/min
P_s	Supply pressure
$\bar{P}$ P/ P_r	dimensionless pressure
μ^*	Equivalent viscosity of the two-phase lubricant
μ_o	Viscosity for pure oil
c	Volume concentration of the particles
ρ_p	Particle density
ρ_o	Oil density
λ	Weight concentration of solid particle
Γ (λ)	New viscosity function for Einstein formula
$S = \rho \Omega^2 R^2 / P_r$	centrifugal parameter
$\bar{Q} = \mu Q / \pi R^3 P_r$	dimensionless volumetric flow rate
$\bar{W} = W/ \pi R^2 P_r$	dimensionless load capacity
m, q, K_Q	Compensator flow constant
$K_P = P_r / P_S$	ratio between inlet pressure and supply pressure

11. References:

[1] .A. Christ and M. Peron. 1980, " Hydrostatic thrust bearing for storage pumps," Escherwyss News, vol. 53 pp. 71.

[2] R. S. Brand, 1956, Journal of Applied Mechanic, vol.77 pp. 363.

[3] Dowson, D., 1961, "Inertia effects in hydrostatic thrust bearings," ASME, Journal of Basic Engineering, vol. 83 pp. 227.

[4] C. Chung, Moon and D. W. Darcing. 1976, " The contribution of fluid film inertia to the thermohydrodynamic lubrication of sector pad thrust bearings," ASME Journal of Lubrication Technology, vol.98, pp.

[5] O. Pinkus and J. W. Land, 1981" Centrifugal effects in thrust bearings and seals under laminar conditions," ASME Journal of Lubrication Technology, vol. 103, pp. 126-136.

[6] R. S. Gupta and V. K. Kapur, 1982, Wear, vol.77 pp. 203.

[7] S. Safar. 1983, " Centrifugal effects in misaligned hydrostatic thrust bearings," ASME Journal of Lubrication Technology, vol.105 pp. 621.

[8] Coombs, J. A. Dowson, D., 1965 "An experimental investigation of the effect of lubrication inertia in hydrostatic thrust bearing," 3rd Lub. And wear conv. Proc. IME, London, U, K. vol. 179 part 3J, P. 96.

[9] V. K. Kapur and K. Verma, (1975) " Energy integral approach for hydrostatic thrust bearing," ASME Journal of lubrication technology vol.97 n.4 pp.697.

[10] Yousif, A. E., and Nacy, S. M., 1981 " Hydrodynamic Behavior of two-phase (liquid-solid) lubricants," Wear, Vol. 66, No. 2, pp.223-240.

[11] Yousif, A. E., and Hassan, K. J., 1985 "The Lubrication of Journal Bearings with two-phase (liquid-solid) lubricants," Proc. Of the JSME Int' l Trib. Conf. Tokyo, pp. 1121-1126.

[12] Khalil, M. F. and Ismail, A. S., "Performance characteristics of externally pressurized bearings under turbulent flow conditions," Sited from ref [6].

[13] Osterele, J. F, and Huges, W. F., 1961" Inertia induced cavitation in hydrostatic in hydrostatic thrust bearings," WEAR, vol. 4 pp. 228.

[14] Khalil, M. F Ismail, A.S. (1989) "Centrifugal effects in externally pressurized bearings under turbulent flow conditions," Tribology International vol.22 n.4 pp. 265-272.

تأثير الاضافات على سلوك المحامل

البرت يوسف نعمان محمد عبد الستار محمد
قسم الهندسة الميكانيكية /كلية الهندسة /جامعة النهرين

الخلاصة

في هذا البحث تم دراسة سلوك المحامل الهيدروستاتيكية ذات مزيتات ثنائية الطور (سائل-صلب) بأضافة الجسيمات الصلبة التي تنثر (تخلط) مع الزيت النقي بتركيز وزني معين وذلك باستخدام معادلة اينشتاين المطورة للزوجة ، مع الاخذ بنظر الاعتبار تأثير القوة الطاردة المركزية الناتجة من دوران المحمل بسرع عالية. كما تمت دراسة تأثير الابعاد الهندسية للمحمل على (الضغط، معدل الجريان، سعة التحميل، اجهادات القص، الطاقة اللازمة والصلابة).

لوحظ من خلال النتائج النظرية زيادة في الحمل بمقدار (8,3 %) عند نسبة التركيز الوزنية (16%) لجسيمات الجرافيت بالمقارنة مع الحمل في حالة عدم وجود الجسيمات الصلبة (زيت نقي) وزيادة في اجهاد القص.